Proceedings of the 2018 IEEE
International Conference on Robotics and Biomimetics
December 12-15, 2018, Kuala Lumpur, Malaysia

Design of a locust-inspired miniature jumping robot

Yaolei Shen, Wenjie Ge*, Xiaojuan Mo, Zhenghang Hou,
Wenbin Song, Yifei Chen, Shaofeng Jin
School of Mechanical Engineering
Northwestern Polytechnical University
Xi′an, China

***Abstract*— The dispersion of landing place and the explosion of motion can make jumping robot work well in unstructured terrestrial environments. Inspired by locusts, we designed a miniature jumping robot based on six-bar mechanism. By theoretical analysis and prototype experiments, we verified the robot shares the similar posture with locusts in take-off phase, which makes it jump stably.**

I. INTRODUCTION

Up to now, terrain mobile robots can be generally divided into four types, including wheeled, snake-like, walking, and jumping robots. Compared with other locomotion types, jumping robots are mainly based on simple mechanical structure with fewer drivers, and have strong ability to overcome obstacles [1]. For these reasons, jumping robots can be applied in rescue, investigation and other fields that need to work in unstructured environments.

In order to improve the performance of jumping robot, including jumping height, distance, stability, and energy utilization, we can get inspiration from the locomotion of animals. Over hundreds of millions of years of evolution, locusts have gradually adapted to unstructured environments with combination of three different locomotion models, walking, jumping and flying. In this paper, we considered the excellent jumping ability of locusts and try to design a system to mimic it.

By mimicking locusts contracting extensor muscle to extend the tibiae, Lambrecht et al designed the Mini-Whegs [2], which can jump 18 cm high. With the same mechanism, Nguyen and Park designed a robot that can jump 71 cm high [3]. Kovac et al designed EPFL 7g jumping robot based on four-bar mechanism, which can jump 1.4 m high [4]. Zaitsev et al used torsional spring to mimic the semi-lunar processes of locusts, which makes TAUB robot jump 3.2 m high [5].

The existed locust-inspired jumping robots mainly focus on mimicking the jumping function of locusts while ignoring the morphological similarity to hindlegs of locusts during take-off.

We used six-bar mechanism with special length ratios to mimic the motion of femur, tibiae, tarsus in hindlegs of locusts. By the coordination of body and jumping leg, the robot can jump stably.

*This work was supported by National Training Programs of Innovation and Entrepreneurship for Undergraduates, China.

II. JUMPING MECHANISM OF LOCUST

A. Take-off phase of locust

A locust can be divided into three subsections: the head, chest and abdomen. The hind limb fixed on the chest is an important part for locusts to jump, which consists of coxa, femur, tibiae, and tarsus. The coxa can flex/extend and adduct/abduct the femur with two pairs of muscle [6]. The femur is thick and almost occupied by the extensor muscles [7]. The tibiae is as long as the femur, but much thinner [7]. And the strong grasping ability of tarsus helps locusts adapt to both smooth and tough surface [8].

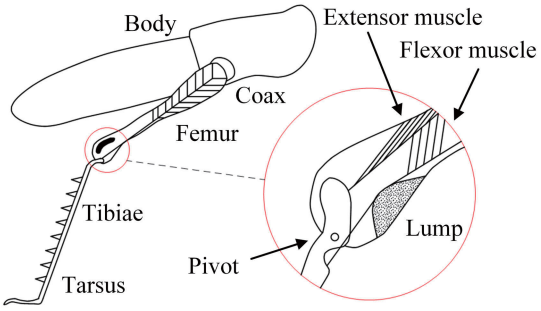

Fig. 1. Structure of the locust hind limb

The take-off phase of locust can be divided into three stages: initial flexion of the tibiae, co-contraction of flexor and extensor muscles, and extension of the tibiae [9]. At co-contraction stage, locusts store energy for jumping via contracting the extensor muscles and semi-lunar processes [10]. In the meanwhile, the structure of knee joint gives the flexor muscles great mechanical advantage, which allows the flexor tension to resist the larger extensor tension [7]. By inhibiting flexor muscles stimulation, the flexor muscles can be relaxed, which allows tibiae to extend under the action of extensor muscles [9].

B. Adjustment of body posture during take-off

By analyzing the high-speed sequential images of the locust jump, Sutton and Burrows came to the conclusion that the take-off angle of locust jump is parallel to a line drawn from the distal end of tibiae through the proximal end of the femur [11]. But when the take-off angle is large and the initial pitch of body is small or the opposite, the centroid of body will be below or above the thrust vector

978-1-7281-0377-8/18/$31.00 © 2018 IEEE

[12]. In this case, the thrust vector will cause a torque working on the centroid of locust, which makes locust tumble [12]. In order to control tumbling, locusts will contract the dorsal longitudinal muscle between the chest and abdomen to generate an opposing torque during the jump impulse to counterpoise the thrust torque [12].

III. LOCUST JUMPING EXPERIMENT

A. Experimental data

In order to analyze the characteristics of the locust jump, a high-speed camera was used to record the jumping movement of the locust during take-off. The basic parameters of the locust used in the experiment are shown in Table I. The joint angles of hind limb were calibrated as shown in Fig. 2, where $\theta_i (i = 1, 2, \cdots, 5)$ is the angle between tarsus and horizontal, tibiae and tarsus, femur and tibiae, femur and body, body and horizontal. In addition, the angle between the body and the line connected from the body centroid to the hip joint is supposed to be $45°$.

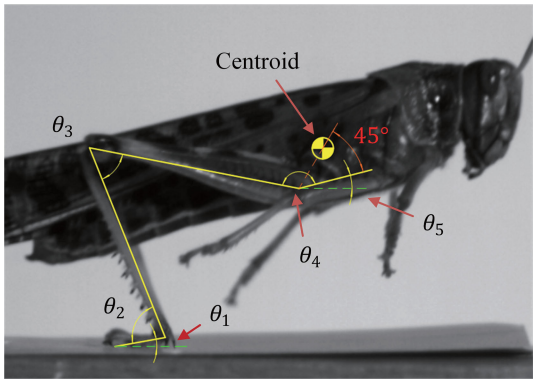

Fig. 2. Calibration of joint angles

TABLE I
BASIC PARAMENTERS OF LOCUST

Item	Body	Femur	Tibiae	Tarsus	Centroid to hip joint
Length (mm)	5.14	21.30	20.45	5.22	3.59
Mass (mm)	0.100	0.045	0.009	0.003	–

TABLE II
THE JOINT ANGLES DURING TAKE-OFF

Time	θ_1	θ_2	θ_3	θ_4	θ_5
0 ms	4.87°	46.56°	20.54°	150.50°	8.34°
4 ms	3.77°	43.02°	12.02°	143.70°	9.06°
8 ms	2.81°	43.21°	10.81°	140.23°	10.18°
12 ms	2.00°	47.14°	16.93°	140.09°	11.71°
16 ms	1.34°	54.80°	30.37°	143.26°	13.65°
20 ms	0.83°	66.19°	51.12°	149.77°	15.99°
24 ms	0.47°	81.32°	79.19°	159.59°	18.75°
28 ms	0.25°	100.18°	114.58°	172.75°	21.91°
32 ms	0.18°	122.77°	157.29°	189.22°	25.48°

The experimental data of joint angles is given in Table II. In order to observe the variation trend of the joint angles during take-off, the data measured were fitted by cubic polynomial fitting, and the results are shown in Fig. 3.

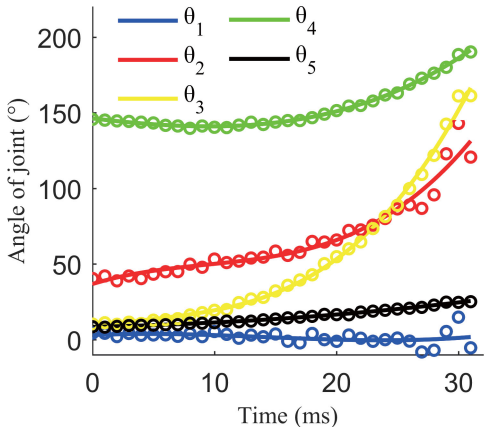

Fig. 3. Joint angles during take-off process

B. Kinematic analysis of take-off phase

For understanding the kinematic characteristics of the locust jump, D-H method was used to build the transformation matrix of each part of the hind limb relative to the horizontal, and the position and posture of the hind limb and body in the ground reference system were obtained. The transformation matrixs between bars are shown at Eq. 1, where C denotes cos , S denotes sin, θ_C is the angle between femur and the line connected from the body centroid to the hip joint, and $l_i (i = 0, 1, 3, 4)$ is the length of tarsus, tibiae, femur and the distance from the centroid of body to the hip joint.

$$ {}^{0}_{1}T = \begin{bmatrix} C(\theta_1(t)) & -S(\theta_1(t)) & 0 & l_1 \cdot C(\theta_1(t)) \\ S(\theta_1(t)) & C(\theta_1(t)) & 0 & l_1 \cdot S(\theta_1(t)) \\ 0 & 0 & 1 & 0 \\ 0 & 0 & 0 & 1 \end{bmatrix} $$

$$ {}^{1}_{2}T = \begin{bmatrix} -C(\theta_2(t)) & -S(\theta_2(t)) & 0 & -l_2 \cdot C(\theta_2(t)) \\ S(\theta_2(t)) & -C(\theta_2(t)) & 0 & l_2 \cdot S(\theta_2(t)) \\ 0 & 0 & 1 & 0 \\ 0 & 0 & 0 & 1 \end{bmatrix} $$

$$ {}^{2}_{3}T = \begin{bmatrix} -C(\theta_3(t)) & S(\theta_3(t)) & 0 & -l_3 \cdot C(\theta_3(t)) \\ -S(\theta_3(t)) & -C(\theta_3(t)) & 0 & l_3 \cdot S(\theta_3(t)) \\ 0 & 0 & 1 & 0 \\ 0 & 0 & 0 & 1 \end{bmatrix} $$

$$ {}^{3}_{4}T = \begin{bmatrix} -C(\theta_c(t)) & -S(\theta_c(t)) & 0 & -l_4 \cdot C(\theta_c(t)) \\ S(\theta_c(t)) & -C(\theta_c(t)) & 0 & l_4 \cdot S(\theta_c(t)) \\ 0 & 0 & 1 & 0 \\ 0 & 0 & 0 & 1 \end{bmatrix} $$

$$ {}^{0}_{i}T = {}^{0}_{1}T \cdot {}^{1}_{2}T \cdots {}^{i-2}_{i-1}T \cdot {}^{i-1}_{i}T \quad (i = 1, 2, 3, 4) \qquad (1) $$

The posture of locust during take-off was calculated, as shown in Fig. 4. It was found that the trajectory of the body centroid was a straight line during take-off phase. But the line deflects at the end of the trajectory, for the tarsus of the locust has left the ground at that time. Therefore, it is necessary to modify the calculated posture.

According to the vertical acceleration expression of the body centroid, as shown at Eq. 2, when the acceleration of the centroid is equal to the gravitational acceleration, the ground has no power to the locust, this moment is the time when the tarsus loses contact with the ground. And the vertical acceleration is calculated in Eq. 3, where $h_{centroid}$ is the height of body centroid in the ground reference system T_0.

$$m_{body} \cdot a_{y-body} = F_{y-groud} - m_{body} \cdot g \tag{2}$$

$$a_{y-body} = \frac{d^2 h_{centroid}}{dt^2} \tag{3}$$

According to the calculation, the locust released the tibiae at 4.1 ms, and at 24.3 ms the tarsus left the ground. In addition, it can be found that the acceleration of body increases slowly and then decreases rapidly at fig. 5, this is consistent with the variation trend of the ratio of the extensor muscle arm to the tibiae length during take-off [7].

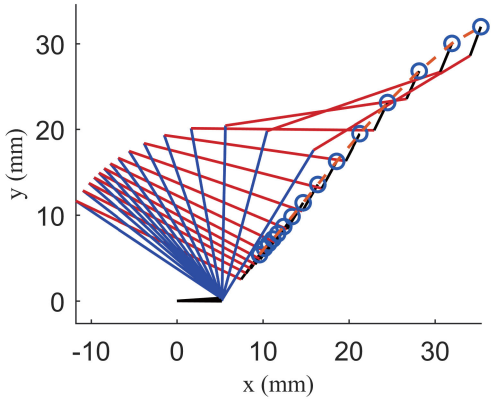

Fig. 4. Posture of locust during take-off

C. Cause of tumbling

In the experiment, we found that the locust tumbled head-upward in the jump process. This phenomenon makes the locust jump direction uncontrollable which leads to inefficiencies of locomotion. Therefore, it is necessary to analyze the cause of tumbling.

If the effect of air is ignored, only gravity will affect the locust after it leaves the ground. And gravity can be seen as directly working on the centroid of locust, which has no torque working on the locust. As the torque formula Eq. 4 show, the rotating trend of the locust will not change when the tarsus has no contact with the ground. So, the rotating trend of the locust is determined by the angular momentum of each part of the locust at the moment when the locust leaves the ground.

$$T = J\frac{d\omega}{dt} \tag{4}$$

In order to analyze the impact of each part on the locust tumbling, the angular momentum of each part relative to the centroid of locust during take-off was calculated. In the

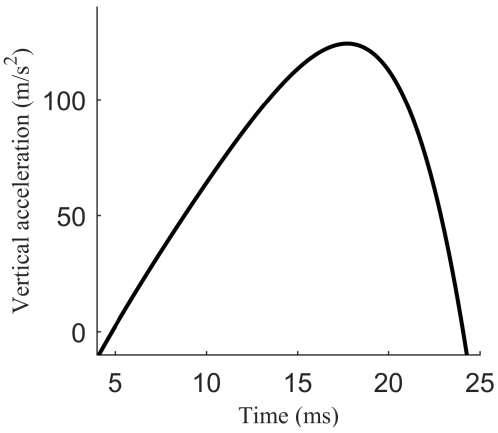

Fig. 5. The vertical acceleration of body centroid during take-off

calculation, each part is assumed to be a homogeneous round rod with corresponding length and mass, that is, the centroid of each part lies at its geometric center, and the rotational inertia relative to its centroid J_i is expressed as Eq. 5. The centroid of locust is determined by its posture, the expression is shown as Eq. 6. And the expression of angular momentum of each part relative to the centroid of locust L_i is shown as Eq. 7, where ω_i is the angular velocity of tarsus, tibiae, femur and body in the ground reference system, x_i and y_i are the horizontal and vertical coordinates of each part in the ground reference system, v_{xi} and v_{yi} is the moving velocity of the centroid of each part.

$$J_i = \frac{1}{12} m_i l_i^2 \tag{5}$$

$$\begin{cases} x_{centroid}(t) = \frac{\sum_{i=1}^{4} m_i x_i(t)}{\sum_{i=1}^{4} m_i} \\ y_{centroid}(t) = \frac{\sum_{i=1}^{4} m_i y_i(t)}{\sum_{i=1}^{4} m_i} \end{cases} \tag{6}$$

$$L_i = \begin{bmatrix} x_i - x_{centroid} \\ y_i - y_{centroid} \\ 0 \end{bmatrix} \times \begin{bmatrix} v_{xi} - v_{x-centroid} \\ v_{yi} - v_{y-centroid} \\ 0 \end{bmatrix} + J_i \begin{bmatrix} 0 \\ 0 \\ \omega_i \end{bmatrix} \tag{7}$$

The angular momentum of each part relative to the centroid of locust during take-off was obtained after calculation, as shown in Fig. 6. It can be seen that the angular momentum of tarsus and tibiae are similar in magnitude, and opposite in direction. This means the effects of tarsus and tibiae on the rotation of the locust cancel each other out. On the contrary, there is a large positive angular momentum in both body and femur at the moment when the locust leaves the ground, which directly related to the locust head-upward tumbling.

In order to make the locust jump more stably, we can add the posture adjustment mechanism. That is, letting the locust to contract the dorsal longitudinal muscle to rotate the abdomen forward during take-off [12], then the angular momentum of the abdomen will reduce the adverse effects of the rotation of body and femur. This provides an effective method for posture balance of jumping robot.

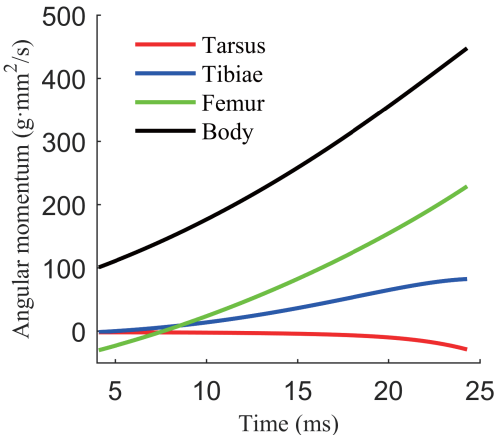

Fig. 6. Angular momentum of each part relative to the centroid of locust

IV. DESIGN OF BIONIC JUMPING MECHANISM

A. Mechanism design

The goals of the robot mechanism design are mimicking the movement of femur, tibiae and tarsus, and adding posture adjustment mechanism during take-off phase. In addition, the structure of locust knee joint should be mimicked to achieve similar jumping mechanics characteristics to locusts.

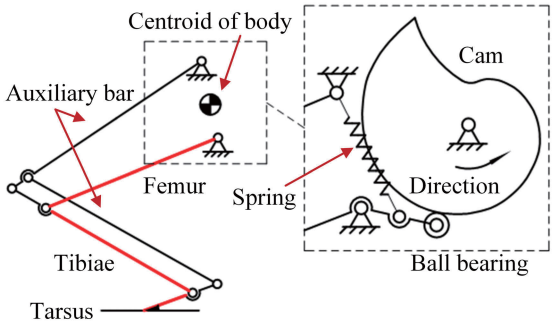

Fig. 7. Jumping mechanism movement diagram

To achieve the goals above, the mechanism is designed as shown in Fig. 7. Before jumping, the cam rotates counter-clockwise to bend the femur and to stretch the spring. When the cam rotates to the highest point, the femur releases and rotates around the body under the spring tension. Because of the two auxiliary bars, the tibiae and tarsus will rotate according to a certain rule. Finally, the robot takes off by kicking the ground with its leg.

To speed up the process of designing, the components listed in Table III were used to build the virtual prototype of jumping robot in CAD software, as shown in Fig. 8.

B. Analysis of jumping performance

Lagrange method was used to establish dynamic equation of the robot, and the joint angles and the acceleration of robot body during take-off phase were obtained after solving the equation. By comparing with the experimental data of the locust, the biological similarity of the jumping robot during take-off phase was analyzed.

TABLE III
BASIC PARAMETERS OF ROBOT COMPONENTS

Components		Material	Weight (g)	Length (mm)	Rotation intertia (kg· mm^2)
body	Frame	UV-curing resin	10	-	35.53
	Axles	Steel	9		
	DC motor	-	13		
	Worm	Copper alloy	10		
	Worm gear	Copper alloy	14		
	Cam	UV-curing resin	4		
	Battery	-	21		
	Bearings	Steel	2		
	Springs	Steel	5		
	Screw	Steel	4		
Femur auxiliary bar		UV-curing resin & C-BAR	3	70	1.86
Femur	Bar	UV-curing resin & C-BAR	4	57	2.98
	Bearings	Steel	1		
	Axles	Steel	1		
Tibiae auxiliary bar		UV-curing resin	2	66.5	0.85
Bar of Tibiae		UV-curing resin	3	64	1.15
Tarsus		UV-curing resin & C-BAR	2	65.5	0.49
Total components		-	108	-	-

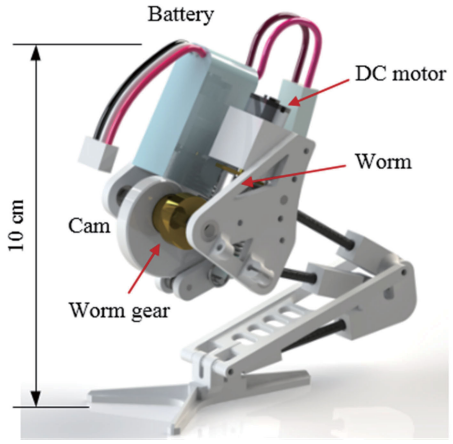

Fig. 8. Virtual prototype of jumping robot

$$\frac{d}{dt}\left(\frac{\partial(T-V)}{\partial\dot{\theta}_1}\right)-\frac{\partial(T-V)}{\partial\theta_1}=0 \tag{8}$$

$$\begin{cases} T=\sum_{i=1}^{5}\frac{1}{2}m_i v_i^2+\frac{1}{2}J_i\omega_i^2 \\ V=\sum_{i=1}^{5}m_i g h_i+\frac{1}{2}k\Delta l^2 \end{cases} \tag{9}$$

If the tarsus of robot does not slip on the ground during take-off, it can be considered that the tarsus is firmly attached to the ground. And the robot can be regarded as a single-degree-of-freedom rigid body system during take-off. Taking the angle between tibiae and ground θ_1 as the generalized coordinate of the system, the dynamic equation of the robot during take-off Eq. 8 was established. To simplify the calculation, the robot system was supposed as a plane linkage

model. In the model, the centroid of each bar at robot leg is located at its midpoint, and the centroid of body is located at the midpoint of the line connecting the two hinges on the frame. Then the T and V in Eq. 8 can be expressed as Eq. 9, where the mass of each rigid body m_i and the rotational inertia relative to its centroid J_i are shown in Table III, v_i and h_i respectively denote the moving speed and vertical direction coordinates of the centroid of each rigid body in the ground coordinate system, ω_i denotes the angular velocity of each rigid body in the coordinate system of the ground, k is the spring stiffness, and Δl is the elongation of the spring.

$$\ddot{h}_{body} = \frac{d^2 h_{body}(\theta_1)}{d\theta_1^2} \cdot \dot{\theta}_1^{\,2} + \frac{dh_{body}(\theta_1)}{d\theta_1} \cdot \ddot{\theta}_1 \qquad (10)$$

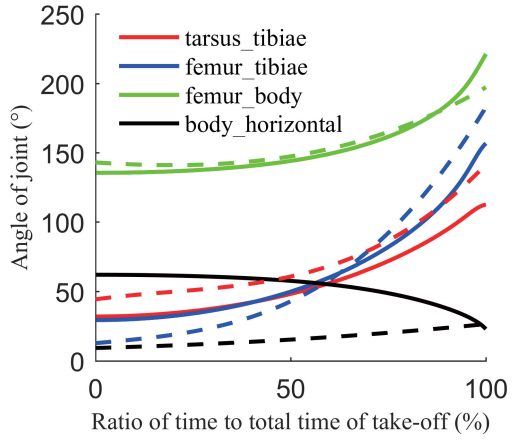

Fig. 9. Joint angles during take-off phase. Solid line is the numerical solution of robot, dotted line is the data from locust experiment.

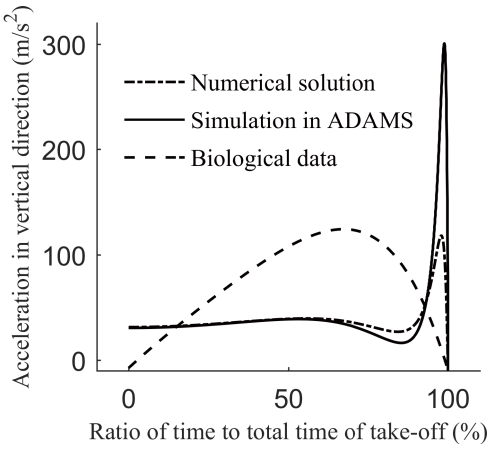

Fig. 10. Vertical acceleration of the body of robot and locust

By numerical method, the dynamic equation was solved with the initial conditions, $\theta_{1-initial}$ is 12° and $\omega_{1-initial}$ is 0 rad/s. Fig. 9 shows the comparsion between the calculated results of the joint angles and the biological data during take-off phase. And Fig. 10 is the acceleration of the centroid of robot body in the vertical direction during take-off.

Comparing the two sets of data in Fig. 9, the variation range and variation trend of robot and locust are similar in the three joint angles between tibiae and tarsus, femur and tibiae, femur and body. But compared with the locust, the angle between the robot body and horizontal decreases rapidly at the late stage of take-off. The decrease of the angle means the robot body rotated in negative direction during take-off. This negative rotation of robot body makes the robot have an additional negative angular momentum, which helps robot overcome the positive rotating trend casued by the rotation of femur and femur auxiliary bar during take-off.

In Fig. 10, the dash dot line is the numerical solution of the dynamic equation, the solid line is the simulation result of the virtual prototype in ADAMS, and the dotted line is the experimental results of locust jump. In the early stage of take-off, the vertical acceleration of robot body stabilises at about 40 m/s^2, and before the robot leaves the ground, the acceleration increases rapidly to a large value and then decreases rapidly. This is not quite similar as the locust during take-off.

C. Jumping simulation

With the simulation of virtual prototype, the jumping performance of the robot was analyzed. Fig. 11 shows the jumping process of the prototype at simulation, the take-off angle at the moment when the robot leaves the ground is 70.64°, and the maximum height of body centroid is 31.1 cm. It can be found that the robot does not rotate at all during flight phase, which verifies the stability of the jumping robot.

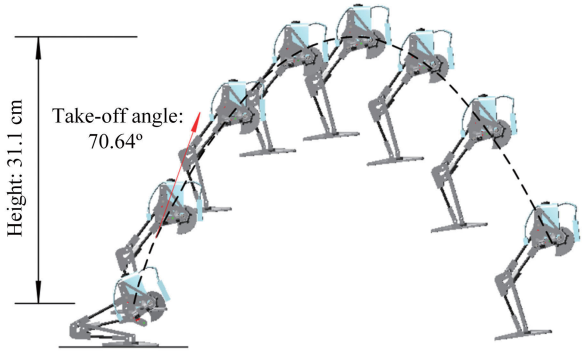

Fig. 11. Jumping simulation of virtual prototype

V. JUMPING EXPERIMENT OF PHYSICAL PROTOTYPE

In order to verify the feasibility of the jumping mechanism design, and to obtain the jumping performance of the robot, a physical prototype was made for jumping experiment. A high-speed camera was uesd to record the jumping process of the robot. By analyzing the high-speed images of the robot jump, the position and posture of robot were obtained.

Fig. 12 shows the two jump processes of physical prototype. Foamed plastic and nylon was respectively used as jump surface at Jump 1 and Jump 2. As the jump image shows, the vertical distance between the tarsus and ground can reach 40 cm when the robot moves to the maximum height, which means that the robot can overcome an obstacle at a height of 40 cm.

The line between body centroid and tarsus centroid was used to record the angular variation of robot body during

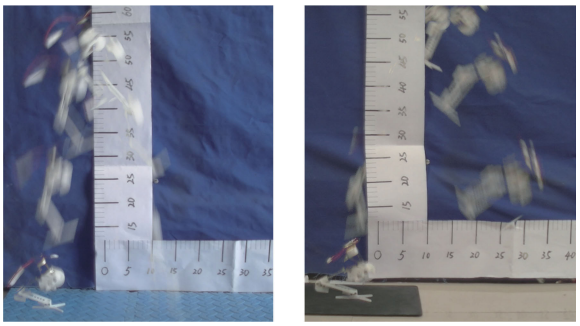

Fig. 12. Jumping experiment of physical prototype

jump processes. Fig. 13 shows the variation of the angle between the line and ground during jump processes of physical and virtual prototype. It can be found the change of robot body angle at Jump 1 was about 30° and about 60° at Jump 2, which proves the negative rotation of the body has a beneficial effect on the stability of the robot. And the differences between the two jumps show that the material of jump surface can affect the rotation of robot during jump.

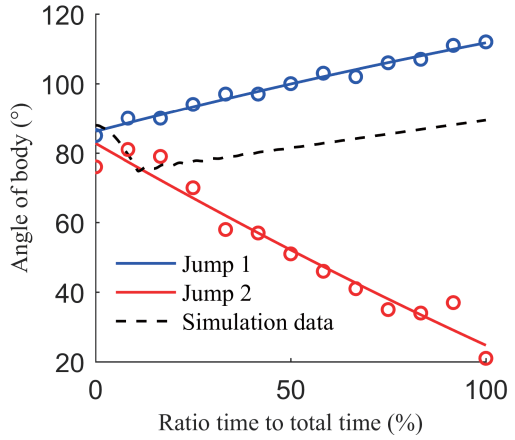

Fig. 13. Angle of body during jump processes

Fig. 14 shows the trajectory of robot body during jump processes of physical and virtual prototype. It can be found that the three curves still have some differences. By taking the derivative with the curves, the take-off angles of physical prototype were obtained, the Jump 1 was 83.74° and Jump 2 was 79.38°. Besides, the distance and height of Jump 2 was both larger than Jump 1, which means the material of jump surface can affect the take-off angle and the energy efficiency of robot jump. And due to the fact that the simulation cannot fully simulate the contact between the robot tarsus and the ground, the mass distribution and the influence of some environmental factors, the simulation results cannot match the experimental results well.

VI. CONCLUSION AND FUTURE PROSPECT

By mimicking the movement of femur, tibiae and tarsus in hindlegs of locusts, a biomimetic jumping robot was designed. And it is proved that the robot can overcome an

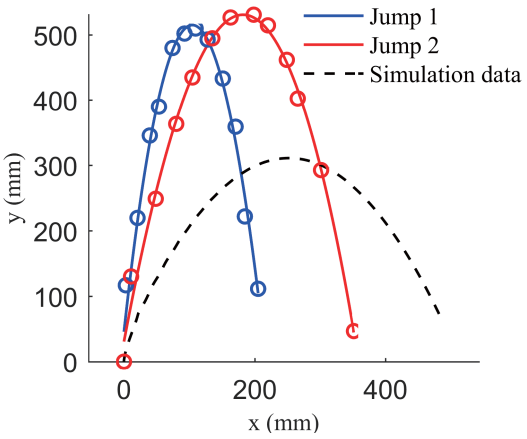

Fig. 14. Trajectory of robot body during jump

obstacle at a height of 40 cm. In addition, posture adjustment mechanism was added during take-off phase of the robot jump, that is, using the negative rotation of robot body to overcome the tumbling trend caused by the rotation of femur and femur auxiliary bar. And the stability of the robot jump was verified with experiments.

In the future work, we consider reducing the weight of the robot and designing a tarsus that meets the biological characteristics to improve the long jumping ability and landing stability of the robot. In addition, more reasonable installation position of energy storage elements will be considered to improve the dynamic biological similarity.

REFERENCES

[1] P. Fiorini and J. Burdick, The development of hopping capabilities for small robots, Auton. Robots, vol. 14, no. 2-3, pp. 239-254, 2003.

[2] B. G. A. Lambrecht, A. D. Horchler, and R. D. Quinn, A small, insect-inspired robot that runs and jumps, Proc. - IEEE Int. Conf. Robot. Autom., vol. 2005, no. April, pp. 1240-1245, 2005.

[3] Q. V. Nguyen and H. C. Park, Design and Demonstration of a Locust-Like Jumping Mechanism for Small-Scale Robots, J. Bionic Eng., vol. 9, no. 3, pp. 271-281, 2012.

[4] M. Kova, M. Fuchs, A. Guignard, J. C. Zufferey, and D. Floreano, A miniature 7g jumping robot, Proc. - IEEE Int. Conf. Robot. Autom., no. c, pp. 373-378, 2008.

[5] V. Zaitsev, O. Gvirsman, U. Ben Hanan, A. Weiss, A. Ayali, and G. Kosa, A locust-inspired miniature jumping robot, Bioinspir. Biomim., vol. 10, no. 6, p. 066012, 2015.

[6] D. Chen, J. Yin, K. Zhao, W. Zheng, and T. Wang, Bionic mechanism and kinematics analysis of hopping robot inspired by locust jumping, J. Bionic Eng., vol. 8, no. 4, pp. 429-439, 2011.

[7] W. J. Heitler, The locust jump, J. Comp. Physiol., vol. 89, no. 1, pp. 93-104, 1974.

[8] Y. Jiao, S. Gorb, and M. Scherge, Adhesion measured on the attachment pads of Tettigonia viridissima (Orthoptera, insecta)., J. Exp. Biol., vol. 203, no. Pt 12, pp. 1887-1895, 2000.

[9] W. J. Heitler and M. Burrows, The locust jump I. The motor programme, J. Exp. Biol., vol. 66, no. 1, pp. 203-219, 1977.

[10] M. Burrows, Development and deposition of resilin in energy stores for locust jumping, J. Exp. Biol., vol. 219, no. 16, pp. 2449-2457, 2016.

[11] G. P. Sutton and M. Burrows, The mechanics of elevation control in locust jumping, J. Comp. Physiol. A Neuroethol. Sensory, Neural, Behav. Physiol., vol. 194, no. 6, pp. 557-563, 2008.

[12] D. Cofer, G. Cymbalyuk, W. J. Heitler, and D. H. Edwards, Control of tumbling during the locust jump, J. Exp. Biol., vol. 213, no. 19, pp. 3378-3387, 2010.